Gondwana Research xxx (2013) xxx–xxx

Contents lists available at SciVerse ScienceDirect

Gondwana Research

journal homepage: www.elsevier.com/locate/gr

Petrogenesis of synorogenic high-temperature leucogranites (Damara orogen, Namibia): Constraints from U–Pb monazite ages and Nd, Sr and Pb isotopes

A. Paul [a,*], S. Jung [a], R.L. Romer [b], A. Stracke [c], F. Hauff [d]

[a] Fachbereich Geowissenschaften, Mineralogisch-Petrographisches Institut, Universität Hamburg, 20146 Hamburg, Germany
[b] Deutsches GeoForschungsZentrum GFZ, Telegrafenberg, D-14473 Potsdam, Germany
[c] Institut für Mineralogie, Westfälische Wilhelms Universität Münster, Corrensstraße 24, 48149 Münster, Germany
[d] GEOMAR Helmholtz Centre for Ocean Research, Wischhofstrasse 1-3, 24148 Kiel, Germany

ARTICLE INFO

Article history:
Received 19 October 2012
Received in revised form 23 May 2013
Accepted 1 June 2013
Available online xxxx

Handling Editor: A.S. Collins

Keywords:
Leucogranites
Crustal melts
Biotite dehydration melting
U–Pb monazite
Sr Nd Pb isotopes

ABSTRACT

Two suites of leucogranites were emplaced at 508 ± 5.9 Ma in the Okombahe District of the Damara belt (Namibia) synchronous with the peak of regional high-temperature metamorphism. The Sr ($^{87}Sr/^{86}Sr_{init}$: 0.707 to 0.711), Nd (εNd_{init}: −4.5 to −6.6), and Pb isotopic ($^{206}Pb/^{204}Pb$: 18.51–19.13; $^{207}Pb/^{204}Pb$: 15.63–15.69; $^{208}Pb/^{204}Pb$: 38.08–38.66) compositions indicate that these peraluminous S-type granites were derived from mid- to lower-crustal rocks, which are slightly different to the metapelitic rocks into which they intruded. Since the leucogranites are unfractionated and show no evidence for assimilation or contamination, they constrain the temperature and pressure conditions of their formation. Calculated Zr and LREE saturation temperatures of ca. 850 °C indicate high-temperature crustal melts. High Rb/Sr and low Sr/Ba ratios are consistent with biotite dehydration melting of pelitic source rocks. Qz–Ab–Or systematics reveal that melting and segregation for the least fractionated samples occurred at ca. 7 kbar corresponding to a mid-crustal level of ca. 26 km. However, there is no evidence for a mantle component that could have served as a local heat source for crustal melting. Therefore, the hot felsic magmas that formed close to the time of peak metamorphism are the result of long-lasting high temperature regional metamorphic conditions and intra-crustal collision.

1. Introduction

Granites are essential components of the continental crust and – in some collision-type orogenic belts – are dominantly the products of crustal anatexis (Collins, 1996). Granites derived from partial melting of older crust carry the geochemical and isotopic signatures of their source and may provide information about the thermal state and composition of the deeper crustal levels. Of special interest are formed granites contemporaneous with peak metamorphism, because these granites potentially preserve evidence for input of mantle material or thermal and tectonic states of lower crustal domains. Furthermore, in deeply eroded orogens without large areas of granulite-grade meta-igneous and metasedimentary rocks, unfractionated igneous rocks provide insights into the geological processes that form the continental crust. In evolved continental crust, generated melts are felsic owing to derivation from mainly meta-pelitic source rocks or extensive melt evolution during ascent. Understanding the processes which generate such felsic melts requires precise information about the source rocks, and the pressure and temperature conditions during melting and melt modification by fractional crystallization and AFC process. Some of this information can be preserved by granites if they do not segregate far from their source and do not undergo substantial modification.

In some orogens there is evidence for either wet melting (Harris et al., 1993; Patiño Douce and Harris, 1998; Guo and Wilson, 2011) or input of mantle melts (Barbarin, 1996; Parada et al., 1997; Soesoo, 2000). In the Damara orogen, leucogranites are likely generated at water-undersaturated conditions and high temperatures during peak metamorphism without direct mantle input (McDermott et al., 1996; Jung et al., 1999; Jung and Mezger, 2001). Resolving the origin of the energy required for intra-crustal melting is an important matter, as internal heating, melting due to metamorphic contact aureoles, or melting due to intrusion of other plutons are all viable and each process reflects different conditions of the continental crust.

The Damara orogen is well suited to study the behavior of felsic melts, because erosion has exposed deep levels of the orogen. This setting will allow identifying the nature of the source, the conditions and reactions during partial melting, which may provide valuable information about the thermal and compositional states of the lower crust.

This study focuses on the genesis of two suites of leucogranites (Figs. 1 and 2) which are situated in the northern part of the high-grade metamorphic Central Damara orogen. We re-investigate two previously studied suites of leucogranites (Haack et al., 1982) and provide additional U–Pb monazite data, new major and trace element data, and Nd and Pb isotope data, the latter obtained on acid-leached

* Corresponding author. Tel.: +49 5525220.
E-mail address: andre-paul@hotmail.de (A. Paul).

1342-937X/$ – see front matter
http://dx.doi.org/10.1016/j.gr.2013.06.008

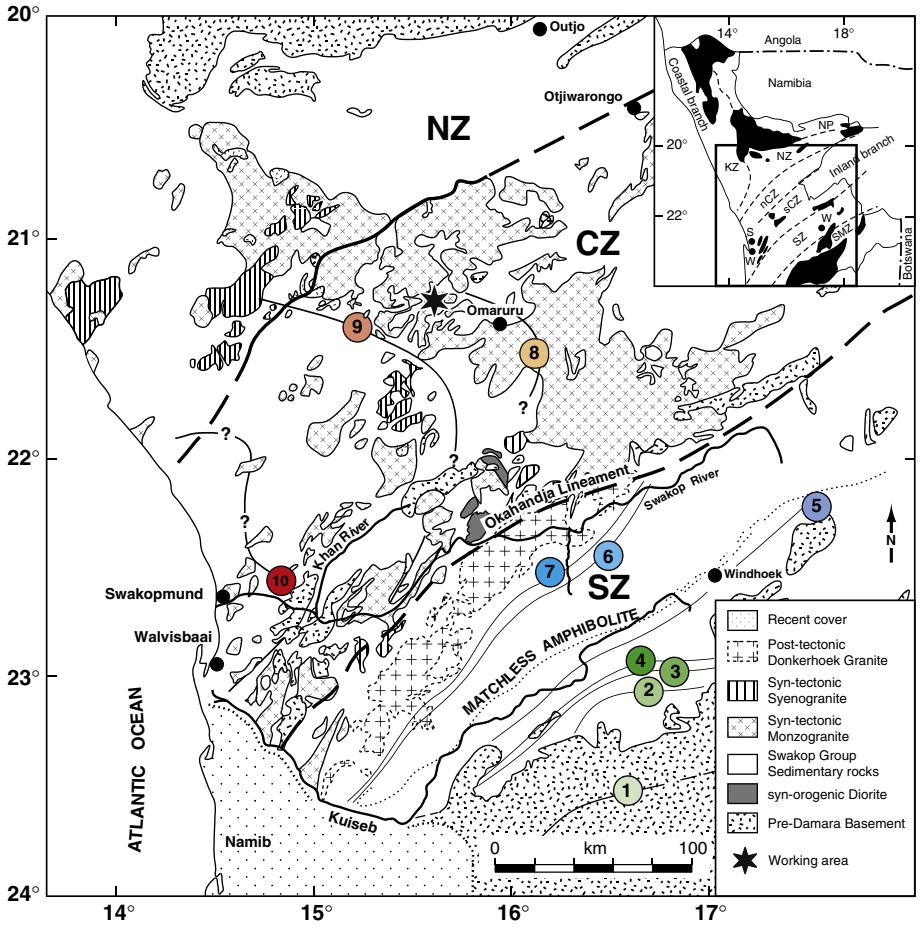

Fig. 1. Generalized geological map showing the study area within the inland branch of the Damara Belt, situated in the northern central zone of the Damara orogen, Namibia. Abbreviations: NZ: Northern Zone, CZ: Central Zone, SZ: Southern Zone. Isograde map displaying the proposed orientation and location of regional metamorphism (Hartmann et al., 1983). Isograds: (1) biotite-in, (2) garnet-in, (3) staurolite-in, (4) kyanite-in, (5) cordierite-in, (6) andalusite ↔ sillimanite, (7) sillimanite-in according to staurolite-breakdown, (8) partial melting due to: muscovite + plagioclase + quartz + H_2O ↔ melt + sillimanite, (9) K-feldspar + cordierite-in, (10) partial melting due to: biotite + K-feldspar + plagioclase + quartz + cordierite ↔ melt + garnet. Abbreviations in inset: KZ, Kaoko Belt; NP, Northern Platform; NZ, Northern Zone; nCZ, northern Central Zone; sCZ, southern Central Zone; SZ, Southern Zone; SMZ, Southern Margin Zone; W, Windhoek; S, Swakopmund.

K-feldspar. The data are used to evaluate the temporal and thermal relationship between granite intrusion and high-grade metamorphism and to place constraints on potential sources and processes.

2. Geological setting

The Y-shaped Neoproterozoic/early Paleozoic Damara orogen is situated between the Congo and Kalahari Craton in Africa and the Rio de la Plata Craton in South America. The orogen comprises three distinct belts, (i) the Kaoko Belt which is trending roughly north–south along the Namibian coast, (ii) the Gariep Belt situated at the southern end trending also north–south towards South Africa, and (iii) the inland Damara Belt (Miller, 1983, 2008) trending NE–SW into Namibia and Botswana. The Pan-African Damara Belt can be subdivided into a northern, central, and southern zone based on stratigraphy, structure, metamorphic grade and geochronology (Miller, 1983). The inland branch of the Damara Belt is oriented in east–northeastern to west–southwestern direction and consists of three zones, the Northern, the Central, and the Southern Zone separated by a major shear zone; the Okahandja Lineament (Fig. 1). Pre-Damara basement gneisses are overlain by a thick metasedimentary layer; the overlying stratigraphic units belong to the Nosib and Swakop groups. The uppermost part of the Swakop group, the Kuiseb Formation, is of particular interest because it is the site where most granites were emplaced.

Samarium–Nd garnet whole rock ages and U–Pb monazite ages obtained on metamorphic rocks of the Central Zone indicate that the orogenic cycle covers a time span from ca. 540 to 490 Ma (Jung and Mezger, 2001, 2003). The duration of igneous activity is less well constrained but apparently covers a similar period from ca. 550 Ma (Jung and Mezger, 2003) to 490 Ma (Jung et al., 2001). Among the intrusive rocks, granites make up more than 90%, the remainder are diorites and tonalites/granodiorites in equal proportions, covering an area of about 75,000 km^2 (Miller, 2008). The deformational phases of the Damara orogen were identified using Rb–Sr whole rock ages of various granites in conjunction with their respective field setting (Haack et al., 1980, 1982). These data imply that the first event (F 1) occurred at 549 ± 22 Ma, followed by a second deformational event (F 2) at 514 ± 22 Ma, corresponding to the peak of metamorphism. Finally, a third deformational event (F 3) occurred between 459 and 479 Ma. Estimates for the peak metamorphic conditions during regional metamorphism indicate high temperatures of 700–750 °C at moderate pressures of 5–6 kbar between 510 and 500 Ma (Masberg et al., 1992; Jung et al., 1998a, 1998b, 2000a, 2000b; Jung and Mezger, 2003). The nearby Oetmoed Granite–Migmatite Complex (Fig. 2) is used as a reference outcrop for the Okombahe district based on the similar appearance of associated high-grade metapelites and leucogranites, and suggests that the peak of high-temperature metamorphism occurred about 505 Ma ago (U–Pb Mnz: 505 ± 2 Ma; Sm–Nd Grt-WR: 508 ± 6 Ma; 511 ± 11 Ma; 505 ± 3 Ma; Jung, 2000; Jung and Hellebrand, 2006) and resulted in partial melting of fertile rocks. The leucogranites studied here are emplaced into high-grade metapelites of the Swakop Group with the metamorphic mineral assemblage cordierite–K-feldspar–sillimanite–

Please cite this article as: Paul, A., et al., Petrogenesis of synorogenic high-temperature leucogranites (Damara orogen, Namibia): Constraints from U–Pb monazite ages and Nd, S..., Gondwana Research (2013), http://dx.doi.org/10.1016/j.gr.2013.06.008

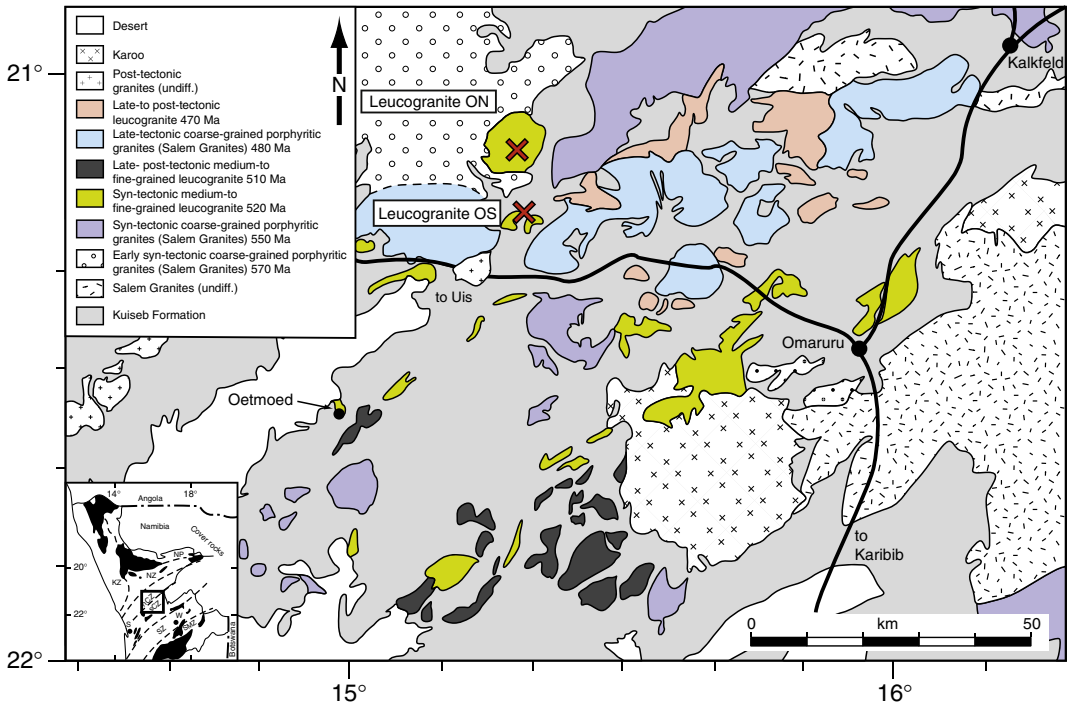

Fig. 2. Detailed geological map showing the location of the plutons within the Northern Central Zone of the Damara orogen, Namibia.

biotite–quartz, but no muscovite (Fig. 3). Preliminary thermometric data (Paul, unpublished) using two new calibrations of the Na-in-Cordierite thermometer (Wyhlidal et al., 2007; Mirwald et al., 2008) yielded temperatures of 725 and 775 °C for two metapelite samples. These temperatures are similar to or higher than pressure–temperature estimates from the Oetmoed Granite–Migmatite complex. Pressure estimates for the metamorphic reaction: bt + sil + qtz <> kfs + crd + H_2O (abbreviations after Kretz, 1983) at 750 °C yielded 4–5 kbar, compatible with pressure estimates from the Oetmoed Granite–Migmatite Complex. $^{40}Ar/^{39}Ar$ thermochronologic data (Gray et al, 2006) in the Central Zone (CZ) of the Damara orogen cluster at about 480–455 Ma.

The granite suites crop out on the Farm Okombahe and are termed Okombahe South (OS) and Okombahe North (ON). From field appearance and investigation of thin sections it is evident that the granite suites are compatible with the definition of leucogranite by Johannsen (1932), for granites with less than 5% mafic minerals. In the field, the

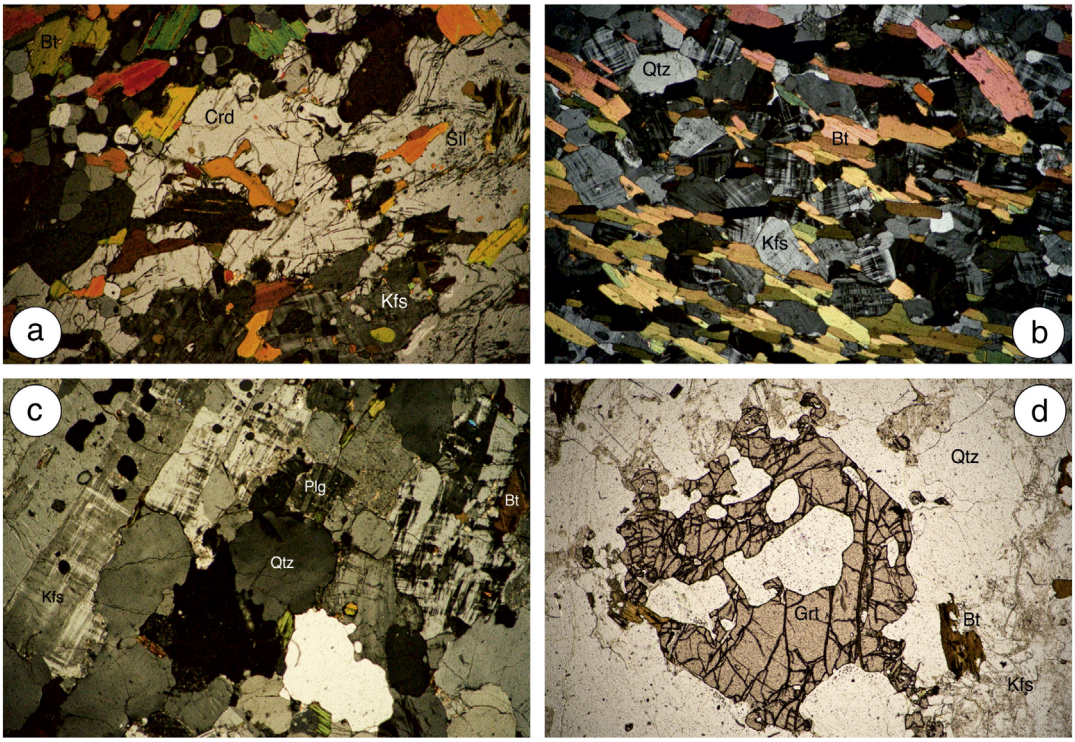

Fig. 3. Microphotographs of (a) high-grade metapelite with crd, kfs, sil and qtz, (b) basement gneiss with kfs, qtz and bt, (c) leucogranite with kfs, pl and qtz and (d) garnet-bearing leucogranite with grt, bt, qtz and kfs. Width of photographs is ca. 2.5 mm.

Please cite this article as: Paul, A., et al., Petrogenesis of synorogenic high-temperature leucogranites (Damara orogen, Namibia): Constraints from U–Pb monazite ages and Nd, S..., Gondwana Research (2013), http://dx.doi.org/10.1016/j.gr.2013.06.008

granites appear undeformed and include randomly distributed, large K-feldspar phenocrysts. The occurrence of inclusion-free, anhedral garnet in the peraluminous granites suggests that garnet crystallized at high temperature, high pressure and low aH_2O (Clemens and Wall, 1988).

3. Petrography of the leucogranites and their country rocks

The granites show a medium grained fabric with no visible foliation. The mineral assemblage consists of K-feldspar/microcline, quartz, plagioclase, biotite (Fig. 3c), some muscovite and abundant euhedral monazite of inferred magmatic origin. In some samples, garnet occurs as a rock-forming mineral phase (Fig. 3d). Garnet forms small anhedral or slightly rounded grains with diameters of 1–5 mm having tiny inclusions of biotite and needle-like apatite and rutile. In some garnet grains the occurrence of larger quartz inclusions is observed. Abundance of biotite is low and generally around or below 5% as estimated from thin sections, but contains a significant number of pleochroic haloes. There is no evidence for post crystallizational deformation. The surrounding country rocks are metapelites and rare basement gneisses.

The most common mineral assemblage in the metapelites is biotite–plagioclase–quartz–K-feldspar–cordierite–sillimanite with accessory tourmaline, apatite, zircon, monazite and Fe–Ti oxides (Fig. 3a). Primary muscovite is absent. Biotite generally defines the foliation. Plagioclase occurs as stubby, idioblastic to subidioblastic grains that are evenly distributed throughout the rock. Quartz ranges from small rounded inclusions in K-feldspar and plagioclase to coarse-grained patches showing undulose extinction. K-feldspar forms large grains; some have subparallel inclusions of biotite. Cordierite is clear, coarse-grained, ovoid to tabular, and may be twinned. It contains inclusions of quartz, tourmaline, biotite and sillimanite. Sillimanite is fibrolitic and may occur as oriented aggregates that, in part, define an earlier foliation. The basement gneiss sample BS 1 is characterized by the assemblage biotite, microcline, quartz and plagioclase (Fig. 3b). Biotite with abundant pleochroic haloes defines the foliation.

4. Analytical techniques

Major and some trace elements (except for Rare Earth Elements; REEs) were determined on fused lithium-tetraborate glass beads using standard XRF techniques at the University of Hamburg. REE abundances of samples S 56, S 57, S 58, S 60, S 62, S 63, S 65, S 66, and S 67 were determined with ICP-AES techniques at the University of Marburg using a Na_2O_2 decomposition, followed by separation using cation exchange columns using 1.75 N HCl and 1.75 N HNO_3 for the extraction of matrix elements, and 6 N HNO_3 and 8 N HNO_3 for extraction of LREE and HREE. The precision is better than 3% for major elements (except for P_2O_5, MnO and Na_2O); generally better than 10% for REE and other trace elements. Accuracy was controlled by the use of several international and in-house standards and the results are in good agreement with recommended values (Jung and Mezger, 2003). The REE analysis of samples S 61, S 72, S 77 and S 78 was carried out via ICP-MS techniques at Actlabs (Canada). Precision is generally better than 10% for the REE relative to the recommended values of the international standard JR-1 which was analyzed as an unknown together with the samples.

For measuring Sr and Nd whole rock isotope compositions, 50 mg of fine powder was digested in concentrated HF-HNO_3 in screw-top Teflon vials in hydrothermal bombs at 180 °C over night. After this treatment, HF was evaporated and the residue was redissolved with 6 N HCl and dried down on a hot plate at 100 °C. Samples were re-dissolved in 2.5 N HCl and centrifuged prior to column chemistry. Strontium and REE were separated by using standard cation exchange columns with a Dowex AG 50W–X 12 resin using 2.5 N HCl for Sr and 6 N HCl for the REE. Neodymium was separated from the other REE by using columns with HDEHP coated Teflon and 0.17 N HCl for Nd. Strontium and Nd isotopes were determined by thermal ionization mass spectrometry (TIMS) at the University Münster using a Finnigan TRITON® operated in static multi-collection. Neodymium isotopes were mass-bias corrected within-run to $^{146}Nd/^{144}Nd = 0.7219$ and strontium isotopes to $^{86}Sr/^{88}Sr = 0.1194$. La Jolla Nd standard measured along with the samples gave $^{143}Nd/^{144}Nd = 0.511856 \pm 3$ (2 S.D.; n = 4) during the measurement period, which agrees well with the long-term reproducibility of 0.511863 ± 3 (2 S.D.). The reproducibility of the Sr standard (NBS 987) is $^{87}Sr/^{86}Sr = 0.710203 \pm 9$ (2 S.D.; n = 4) which is similar to the long-term reproducibility of 0.710207 ± 9 (2 S.D.).

For Pb isotope analyses, high purity feldspar separates were treated with a mixture of 1:1 HCl/HNO_3 at 100–130 °C over night to dissolve surface contaminants and were subsequently washed with ultra-pure water. After this treatment, the feldspar separates were leached three times for 2 min on a hot plate with a mixture of concentrated HF and 6 N HNO_3 (ca. 10:1). After each leaching step, the samples were rinsed several times with ultra-pure water. After dissolution, the samples were evaporated to dryness and converted to chloride using 6 N HCl, centrifuged and loaded on anion exchange resin in chloride form (Mattinson, 1986). Lead isotope analyses were carried out by TIMS using a Finnigan® TRITON at the Westfälische Wilhelms Universität Münster and a Finnigan® MAT 262 at GEOMAR in Kiel. The Pb was loaded on Re single filaments using the H_3PO_4–silica gel method (Cameron et al., 1969). All samples were corrected for mass fractionation of 0.13% per amu.

Monazite was dissolved over night using concentrated H_2SO_4 in Savillex beakers on a hot plate at 220 °C. The samples were taken up in 3 N HCl and loaded on Bio-Rad AG1-X8 ion-exchange resin. Pb was purified using HCl–HBr ion-exchange chromatography, and U was additionally purified using HCl–HNO_3 ion-exchange chromatography (cf. Romer et al., 2005). U and Pb were loaded with H_3PO_4 and silica gel on separate Re single-filament (Gerstenberger and Haase, 1997) and analyzed using a secondary electron multiplier (SEM) and Faraday collectors on a Thermo Triton multi-collector mass-spectrometer at Deutsches GeoForschungsZentrum. Pb^+ was analyzed at 1220 to 1260 °C and UO_2^+ at 1320 to 1360 °C, respectively. Mass fraction was corrected with 0.06% per amu as determined by the repeated measurement of NBS 981 and U010 reference materials.

5. Age of leucogranitic magmatism in the Damara orogen

Four monazite samples from the leucogranites labeled ON were analyzed using U–Pb ID-TIMS. The analytical results are shown in Table 1. All samples have very radiogenic Pb isotopic composition, with measured $^{206}Pb/^{204}Pb$ larger than 5300 (Table 1). Common lead was corrected using the Pb isotopic composition of leached K-feldspar ($^{206}Pb/^{204}Pb = 18.714$, $^{207}Pb/^{204}Pb = 15.689$, $^{208}Pb/^{204}Pb = 38.428$). Using a different Pb isotopic composition for common Pb, e.g., average crustal Pb (Stacey and Kramers, 1975) does not affect the isotopic ratios of radiogenic Pb. Thus, the scatter of the monazite samples in the Concordia diagram (Fig. 4) is not due to the common Pb correction. The monazite U–Pb data fall on or above the Concordia curve (Fig. 4) and define a poorly constrained discordia that intercepts with the concordia at 491 ± 21 Ma (2σ, MSWD = 9.7).

Monazite strongly prefers Th over U. ^{230}Th is an intermediate isotope of the ^{238}U decay series and eventually decays to ^{206}Pb. Monazite incorporates ^{230}Th to a much higher extent than is supported by ^{238}U and, therefore, monazite typically shows excess ^{206}Pb (e.g., Mattinson, 1973; Schärer, 1984). The extent of ^{206}Pb excess depends on the initial contrast of Th/U_{rock} and $Th/U_{monazite}$ and decreases with increasing age of the monazite. Using an age of ca. 500 Ma and the measured $^{208}Pb/^{206}Pb$, the $^{232}Th/^{238}U$ of the monazite samples was calculated. All samples have $^{232}Th/^{238}U$ ranging from 12.2 to 24.6. For such high $^{232}Th/^{238}U_{atomic}$ values, the $^{206}Pb/^{238}U$ and $^{207}Pb/^{206}Pb$ ratios of Paleozoic monazite still are affected by ^{206}Pb excess. The $^{206}Pb/^{238}U$ and $^{207}Pb/^{206}Pb$ ratios were

Please cite this article as: Paul, A., et al., Petrogenesis of synorogenic high-temperature leucogranites (Damara orogen, Namibia): Constraints from U–Pb monazite ages and Nd, S..., Gondwana Research (2013), http://dx.doi.org/10.1016/j.gr.2013.06.008

Table 1
U–Pb analytical results for monazite from the Okombahe area, Damara orogen (Namibia).

Sample[a]	Weight (mg)			Concentrations (ppm)		^{206}Pb	Radiogenic Pb (at%)[c]			Atomic ratios[c]					Apparent ages (Ma)[c]		
		U	Pbtotal	^{204}Pb measured[b]	^{206}Pb	^{207}Pb	^{208}Pb	^{206}Pb / ^{238}U	$^{206}Pb^{d}$ / ^{238}U	^{207}Pb / ^{235}U	^{207}Pb / ^{206}Pb	$^{207}Pb^{d}$ / ^{206}Pb	^{206}Pb / ^{238}U	$^{206}Pb^{d}$ / ^{238}U	^{207}Pb / ^{235}U	^{207}Pb / ^{206}Pb	$^{207}Pb^{d}$ / ^{206}Pb
Leucogranite sample S77																	
Monazite																	
(1)	0.054	2032	1209	6600	12.18	0.69	87.13	.083496	.083436	.653737	.056786	.05683	517	517	511	483	483
									.082548			.05744		511			509
(2)	0.024	2512	869	8760	20.34	1.16	78.50	.081753	.081729	.643289	.057069	.05709	507	506	504	494	495
									.081260			.05742		504			508
(3)	0.063	2206	1516	7750	11.30	0.64	88.06	.089573	.089501	.702326	.056867	.05691	553	553	540	487	489
									.088463			.05758		546			514
(4)	0.138	2507	1208	5330	14.98	0.85	84.17	.083192	.083149	.652904	.056920	.05695	515	515	510	489	490
									.082454			.05743		511			509

[a] Mineral concentrates were obtained using heavy liquids and Frantz isodynamic magnetic separator. Concentrates were purified by hand under the binocular. Monazite was dissolved with concentrated H_2SO_4 in Savillex beakers on a hot plate at 220 °C. Lead and uranium were separated and purified using HBr–HCl ion-exchange chromatography. U and Pb were loaded with H_3PO_4 and silica gel on separate Re single-filament and analyzed using a secondary electron multiplier (SEM) and Faraday collectors. Pb^+ was analyzed at 1220 to 1260 °C and UO_2^+ at 1320 to 1360 °C, respectively, on a Thermo Triton multi-collector mass-spectrometer at Deutsches GeoForschungsZentrum using Faraday collectors and ion-counting.

[b] Ratio corrected for 0.1%/amu mass-discrimination and isotopic tracer. Not corrected for ^{206}Pb excess or deficit (Schärer, 1984).

[c] Corrected for mass-discrimination, isotopic tracer contribution, 15 pg of Pb blank, 1 pg of U blank and initial common Pb ($^{206}Pb/^{204}Pb = 18.714$, $^{207}Pb/^{204}Pb = 15.689$, $^{208}Pb/^{204}Pb = 38.428$) as determined on leached K-feldspar ($HF:HNO_3 = 10:1$, 2–3 min, 3 times) from the same rock sample. Typical 2sigma uncertainties for $^{206}Pb/^{238}U$ and $^{207}Pb/^{235}U$ and correlation between these errors are 0.6%, 0.7%, and 0.99. Apparent ages were calculated using the constants recommended by IUGS ($\lambda^{235}U = 9.8485E-10\ y^{-1}$, and $\lambda^{238}U = 1.55125E-10\ y^{-1}$).

[d] Corrected for ^{206}Pb excess using the Th/U = 5 of the rock (0.4 for the lower row) and the correction-procedure described in Schärer (1984). U and Th on whole-rock samples determined XFA and ICP-MS on <1 mm size powder of the same rock from which monazite was extracted.

corrected for excess Pb using $^{232}Th/^{238}U$ values of 5.0 and 0.4 for the melt from which monazite had crystallized (Table 1). The value of 5.0 corresponds to the measured Th/U of the rock, whereas the value of 0.4 seems to remove the effect of excess ^{206}Pb completely. The correction of excess ^{206}Pb using lower Th/U values results in a higher scatter of the data around the discordia. The discordia defined by the data corrected for Th/U = 5.0 still shows significant excess scatter and intercepts the concordia at 499 ± 32 Ma (2σ, MSWD = 37). In contrast, the discordia defined by the data corrected for Th/U = 0.4 shows a perfect fit and has a well-constrained intercept with the concordia at 508.2 + 5.5/+5.9 Ma (2σ, MSWD = 0.024). Granites typically have Th/U values around 2, although U-rich granites may show distinctly lower Th/U values. In contrast, high Th/U ratios are generally characteristic for mantle-derived rocks (around 3.8–4.2) and in particular high-grade metamorphic rocks

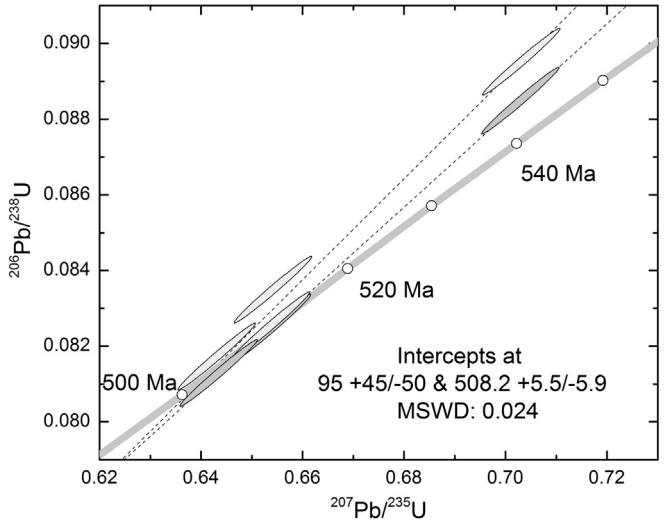

Fig. 4. U–Pb monazite data for leucogranite sample S77 from ON. Data are shown with correction for excess Pb using a Th/U of rock = 5 (light gray ellipsoid), and Th/U of rock = 0.4 (gray ellipsoid).
Data from Table 1.

may reach values > 8, which are uncommon in granites. The high Th/U of the leucogranites ON may reflect loss of U at the surface or the high monazite content (and its extreme Th/U) of the granite. Especially, if monazite got enriched during magma evolution, the Th/U of the granite may not reflect the Th/U of the melt from which the monazite crystallized. Thus, for both explanations, a Th/U lower than 5.0 may be appropriate for the correction of ^{206}Pb excess. A Th/U value of 5.0 for the correction of excess ^{206}Pb underestimates ^{206}Pb-excess. As the discordia through the monazite data yields an older intercept age for a higher correction of ^{206}Pb, the ca. 500 Ma age obtained for Th/U = 5.0 represents a minimum age. The discordia obtained for data corrected for Th/U = 0.4 yields the best fit of the data to a discordia and its intercept at ca. 508 Ma possibly represents the closest estimate of the emplacement age of the granite.

Haack et al. (1980, 1982) reported a Rb–Sr whole rock age of 514 ± 22 Ma for leucogranites from OS and a Rb–Sr whole rock age of 478 ± 27 Ma for leucogranites from ON. Both ages were interpreted as intrusion ages by Haack et al. (1980). The new U–Pb monazite age for sample S 77 from ON, however, is 508 ± 5.9 Ma (Fig. 4). This slightly older age is interpreted to represent the intrusion age as the U–Pb system of monazite in dry systems remains closed to very high temperatures (e.g., Schärer, 1984; Copeland et al., 1988; Rötzler and Romer, 2001) and the dated monazite has a nearly euhedral crystal shape, suggesting a magmatic origin. Although there is a marginal overlap in error between the Rb–Sr whole rock age reported by Haack et al. (1980) and the new U–Pb monazite age, it is quite possible that the Rb–Sr whole rock age is too young and may lack geologic significance either because the major phases biotite and feldspars had behaved as open systems due to alteration or unmixing (e.g., microcline twinning) or the regionally sampled whole rock granite samples a priori did not fulfill the requirements for an isochron. The older U–Pb age obtained for monazite age of the leucogranites from ON implies that these rocks have essentially the same age as peak metamorphism (520–500 Ma; Jung and Mezger, 2003; Jung et al., 1998b, 2000a, 2000b). This older age has important implications for the genetic interpretation of these leucogranites: decompression melting due to uplift of the orogen late in the metamorphic evolution is in conflict with the geochronologic data. In the absence of U–Pb data from the OS granites we

Please cite this article as: Paul, A., et al., Petrogenesis of synorogenic high-temperature leucogranites (Damara orogen, Namibia): Constraints from U–Pb monazite ages and Nd, S..., Gondwana Research (2013), http://dx.doi.org/10.1016/j.gr.2013.06.008

interpret the Rb–Sr age of 514 ± 22 Ma as a minimum age, because similar S-type granites from the Damara orogen also intruded during the time of peak metamorphism at 520–500 Ma (Jung et al., 2000a).

6. Geochemistry

The two leucogranite suites, Okombahe South (OS; samples S 56 to S 65 and OS 1 to OS 4) and Okombahe North (ON; samples S 66 to S 77 and ON 1 and ON 2) have similar contents of major elements (Fig. 5), with SiO_2 ranging from 69.9 to 73.4 wt.%. In both suites high contents of Al_2O_3, K_2O and MnO are observed in the two most primitive samples and constant lower values for higher SiO_2 contents. In contrast, TiO_2, CaO, Fe_2O_3, Na_2O and MgO show no discernible variation with increasing SiO_2. Granites from OS have Rb/Sr between 2.4 and 4.4, Rb/Ba from 0.4 to 1.0 and Sr/Ba of ~0.2. Granites from ON show narrower ranges for these element ratios at similar SiO_2 concentrations (Rb/Sr = 2.3–3.3, Rb/Ba = 0.4–0.7, and Sr/Ba ~0.2).

Both granite suites are weakly peraluminous with alumina saturation indices (ASI) (ASI = molar A/CNK: $(Al_2O_3/CaO + Na_2O + K_2O)$) from 1.04 to 1.09. They are strongly enriched in LREE (Fig. 6 and Table 2), with chondrite-normalized La_n abundances from 203 to 332 in the OS leucogranites and from 412 to 501 in the ON leucogranites. Both granite suites have pronounced negative Eu anomalies (expressed as $Eu/Eu^* = Eu/(\sqrt{(Sm * Gd)}) = 0.30$ to 0.15), which are positively correlated with total REE contents. The enrichment of LREE to HREE, best displayed by chondrite-normalized La_n/Yb_n, allows distinguishing the two suites. For leucogranites from OS, the La_n/Yb_n ranges from 16 to 31 whereas leucogranites from ON have higher La_n/Yb_n between 58 and 96. Both suites are characterized by unusually high U and Th concentrations, between 7 and 13 ppm and from 31 to 64 ppm, respectively, in the leucogranites

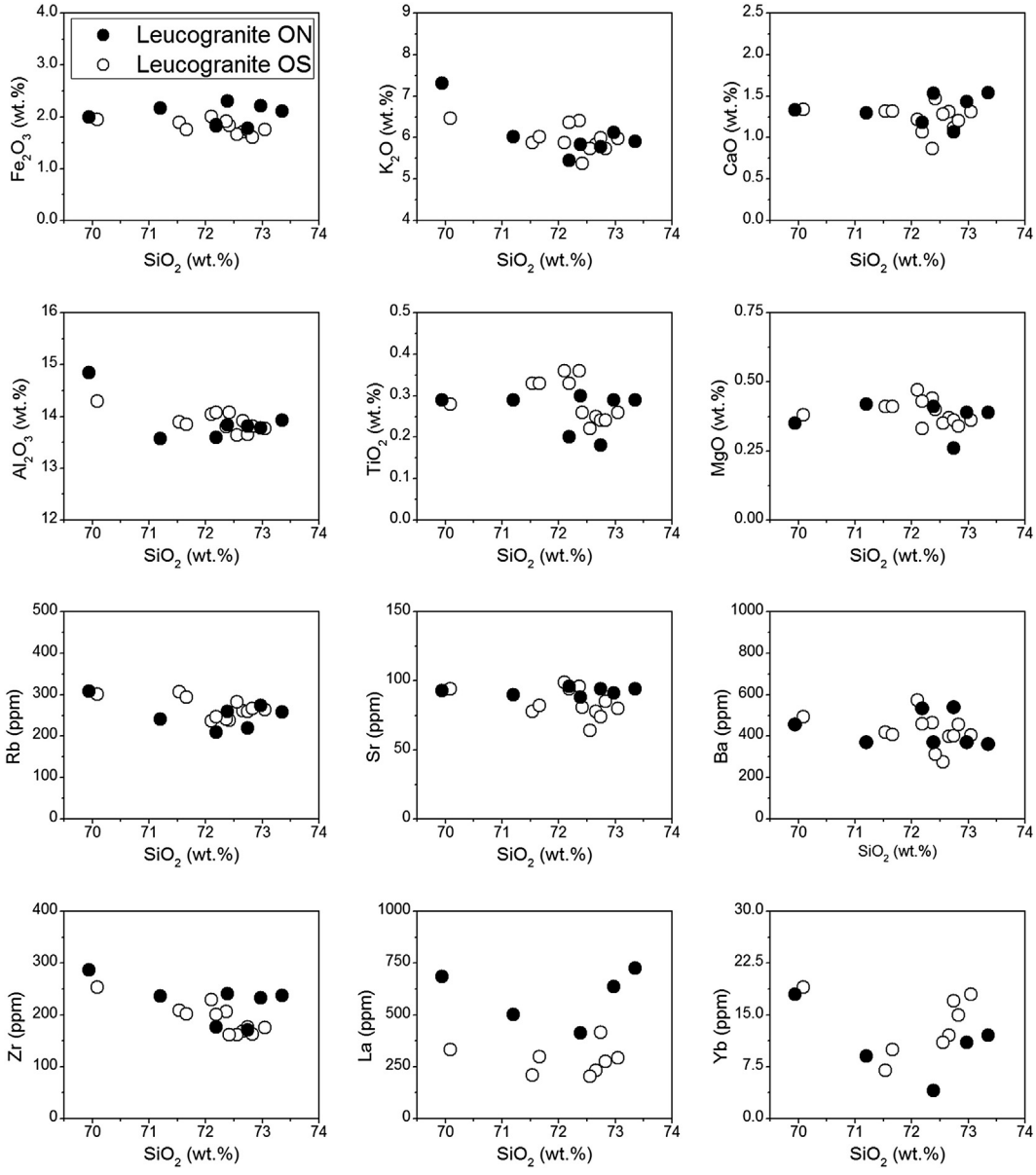

Fig. 5. Major and trace element variation diagram of leucogranites from the Okombahe district, Namibia. Data from Table 2.

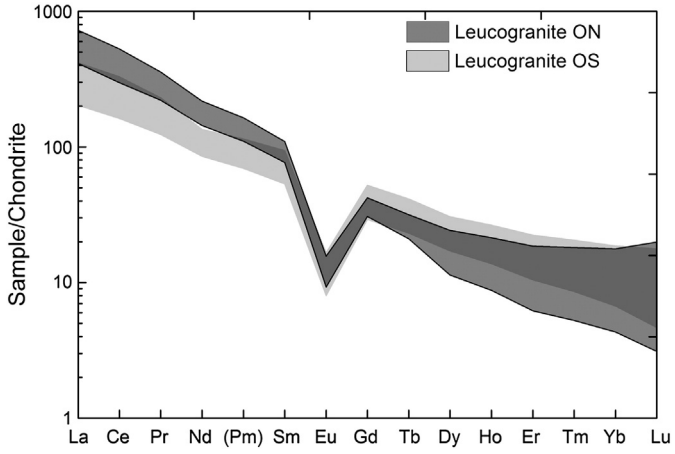

Fig. 6. REE plot of leucogranites from ON and OS. Normalization factors after Boynton (1984). Data from Table 2.

from OS. In the leucogranites from ON, U and Th range from 3 to14 ppm and from 44 to 74 ppm, respectively. The Th/U for OS varies from 2.7 to 5.1, whereas the granites from ON have more variable Th/U from 3.1 to 24. There is no correlation of Th/U with SiO_2 in both suites.

The major and trace element composition of the two metasedimentary rocks and the gneissic basement sample is given in Table 2. The metasedimentary rocks can be classified as Al- and Fe-rich metapelites. They have slightly lower SiO_2 contents (56–58 wt.% SiO_2) and higher Al_2O_3 values (19.1 to 19.6 wt.%) than metapelites from the Oetmoed Granite–Migmatite Complex with 58–60 wt.% SiO_2 (OGMC; Jung et al., 1999). Both metapelite suites have K_2O contents of ca. 4.55 wt.% and Na_2O contents between 0.94 and 1.34 wt.%. FeO/MgO ranges from 1.97 to 1.87, similar to those in metasediments from the Damara orogen. Rubidium and Ba abundances are high (481 ppm and 679 ppm) and the Sr content is moderately low (108 ppm) relative to common metapelites and metagreywackes from the Damara orogen (McDermott and Hawkesworth, 1990; Jung et al., 1999; Masberg et al., 2005).

Results of the Sr, Nd and Pb isotope analyses are given in Table 3. The most notable feature is that both leucogranite suites have rather homogenous isotope compositions (Fig. 7). The OS leucogranites have initial εNd values between −4.5 and −5.3 and initial $^{86}Sr/^{87}Sr_{(508\ Ma)}$ ratios from 0.71041 to 0.71220, whereas the ON leucogranites have initial εNd values from −5.9 to −6.6 and initial $^{86}Sr/^{87}Sr_{(508\ Ma)}$ ratios from 0.70765 to 0.71115 (Fig. 7). Neodymium model ages (calculated following the procedure of Milisenda et al., 1994) use a depleted mantle reservoir ($^{143}Nd/^{144}Nd = 0.513144$, $^{147}Sm/^{144}Nd = 0.222$, Jacobsen and Wasserburg, 1980) and range from 1.5 to 1.7 Ga for the OS leucogranites and from 1.4 to 1.5 Ga for the ON leucogranites. The $^{206}Pb/^{204}Pb$ and $^{207}Pb/^{204}Pb$ compositions (Fig. 8) of acid leached K-feldspars from the OS leucogranites range from 18.51 to 18.60 and 15.63 to 15.67 respectively. For the granites from ON, the $^{206}Pb/^{204}Pb$ ratios range from 18.68 to 19.13 and from 15.68 to 15.69. $^{208}Pb/^{204}Pb$ of the OS leucogranites ranges from 38.08 to 38.13 and for the leucogranites from ON from 38.43 to 38.66. In Pb isotope space both leucogranite suites either plot above (Fig. 8a) or to the right (Fig. 8b) of the two stage U–Pb growth curve of Stacey and Kramers (1975). In $^{208}Pb/^{204}Pb$ vs. $^{206}Pb/^{204}Pb$ space, both suites plot to the right of the Stacey and Kramers (1975) growth curve.

7. Discussion

7.1. Fractional crystallization

Major and trace element composition of the Okombahe leucogranites OS and ON (Fig. 5) suggests that the extent of crystal fractionation is limited. A negative correlation of SiO_2 with K_2O and the lack of correlation of SiO_2 with CaO and Na_2O indicate a dominant role of K-feldspar during fractional crystallization. However, the positive correlation between Sr and Eu/Eu* suggests that plagioclase also fractionated to a limited extent. In both leucogranite suites, LREE abundances decrease with increasing SiO_2, suggesting fractionation of accessory mineral phases such as monazite or apatite (Miller and Mittlefehldt, 1982). In samples from ON, a significant spread in HREE is observed, in conjunction with a negative correlation of Fe + Mg + Ti vs T (°C), resulting from removal of previously accumulated restitic garnet of peritectic origin.

The distinct incorporation of Rb, Sr, and Ba in the key minerals biotite, plagioclase and K-feldspar allows quantitative investigation of the respective roles of these mineral phases during fractional crystallization. The internally consistent set of partition coefficients for Rb, Ba and Sr for the minerals alkali feldspar, plagioclase and biotite from Bea et al. (1994) was used, because the range of SiO_2 of the investigated leucosomes agrees well with that in the granites from Okombahe. The estimated extent of fractional crystallization according to the model is about 25% for the leucogranites from OS and ca. 10% for the leucogranites from ON, consistent with the limited major element variability. Plagioclase and K-feldspar contributed to the fractionating mineral assemblage while biotite only plays a minor role (Fig. 9). The compositions of granites from ON can be accounted for by K-feldspar fractionation alone, which is consistent with the evolution of leucogranites from elsewhere in the Damara orogen (Jung et al., 1999, 2000a, 2009).

7.2. Geochemical constraints on the source of leucogranites

Felsic peraluminous melts, such as the leucogranites from OS and ON, likely form by partial melting of metapelites and metagreywackes under water-undersaturated conditions (Tompson, 1982; Miller, 1985; Le Breton and Thompson, 1988; Vielzeuf and Holloway, 1988; Vielzeuf et al., 1990; Vielzeuf and Montel, 1994; Patiño Douce and Harris, 1998). Enrichment of Ba and Rb relative to Sr, high K_2O (>5.0 wt.%) and moderately low CaO (<1.2 wt.%) contents are indicative for a metasedimentary source (Miller, 1985). For the leucogranites studied here, low Na_2O, CaO and Ba together with high K_2O and moderately high Rb abundances result in high Rb/Sr (>2.4), high Rb/Ba (>0.4) and low Sr/Ba (<0.26) implying a metapelitic source rock that melted at water-undersaturated conditions (Harris and Inger, 1992; McDermott et al., 1996).

Experimental pelite melt compositions by Patiño Douce and Johnston (1991) overlap with those of the leucogranites in Al_2O_3, FeO and MgO vs. SiO_2 space (Fig. 10). In contrast, there is a clear distinction from melt compositions derived by muscovite dehydration melting of metapelites (Patiño Douce and Harris, 1998) (Fig. 10), suggesting that metapelite with abundant biotite rather than muscovite is the likely source rock for the ON and OS leucogranites. This interpretation is compatible with the general absence of muscovite in country rock metapelites implying that muscovite is also absent at deeper crustal levels (Fig 11).

Unradiogenic low initial $^{87}Sr/^{86}Sr$ are observed for both granite suites implying that the source rocks did not have high Rb/Sr. In the leucogranites from OS and ON, Sr and Nd isotope compositions are similar to those of metasedimentary xenoliths and some metasedimentary rocks found in the nearby Oetmoed Granite–Migmatite Complex (OGMC; Jung, 2005). In the OGMC, initial $^{87}Sr/^{86}Sr$ of the metasedimentary xenoliths varies between 0.7082 and 0.7132, compared to $^{87}Sr/^{86}Sr = 0.7104$ to 0.7122 in the OS and 0.7076 to 0.7111 in the ON leucogranites. This relatively narrow range of $^{87}Sr/^{86}Sr$ may be attributed to either homogeneous melts or to sources with similarly low $^{87}Sr/^{86}Sr$.

Comparison of Sr, Nd and Pb isotope data from metasedimentary xenoliths observed in S-type granites from the nearby Oetmoed Granite–Migmatite Complex (Jung, 2005) indicates that the investigated leucogranites are derived from similar metasedimentary source rocks (Figs. 7 and 8). Depleted mantle Nd model ages of 1.5 ± 0.1 Ga of the

Please cite this article as: Paul, A., et al., Petrogenesis of synorogenic high-temperature leucogranites (Damara orogen, Namibia): Constraints from U–Pb monazite ages and Nd, S..., Gondwana Research (2013), http://dx.doi.org/10.1016/j.gr.2013.06.008

Table 2
Major (wt.%) and trace (ppm) element composition of Leucogranites, Metasediments (MS) and Basement gneiss (BS) from the Okombahe district, Namibia.

Sample	S56	S57	S58	S60	S61	S62	S63	S65	OS1	OS2	OS3	OS4	S66	S67	S72	S77	S78	ON1	ON2	BS1	MS2	MS1
SiO_2	72.7	70.1	73.1	72.6	72.7	72.8	71.5	71.7	72.1	72.4	72.4	72.2	71.2	72.4	69.9	73.0	73.4	72.2	72.7	63.9	56.8	58.0
TiO_2	0.25	0.28	0.26	0.22	0.24	0.24	0.33	0.33	0.36	0.26	0.36	0.33	0.29	0.30	0.29	0.29	0.29	0.20	0.18	0.86	0.96	0.9
Al_2O_3	13.9	14.3	13.8	13.6	13.7	13.8	13.9	13.9	14.0	14.1	13.8	14.1	13.6	13.8	14.8	13.8	13.9	13.6	13.8	15.1	19.1	19.6
Fe_2O_3	1.71	1.95	1.75	1.66	1.74	1.60	1.89	1.75	2.01	1.83	1.91	1.84	2.17	2.30	1.99	2.21	2.11	1.82	1.78	7.01	9.92	9.68
MnO	0.03	0.06	0.04	0.04	0.04	0.03	0.03	0.03	0.03	0.02	0.02	0.02	0.04	0.05	0.05	0.05	0.04	0.05	0.04	0.09	0.15	0.1
MgO	0.37	0.38	0.36	0.35	0.36	0.34	0.41	0.41	0.47	0.40	0.44	0.43	0.42	0.41	0.35	0.39	0.39	0.33	0.26	2.19	4.52	4.65
CaO	1.31	1.34	1.31	1.28	1.12	1.20	1.32	1.32	1.22	1.47	0.87	1.07	1.30	1.53	1.33	1.43	1.54	1.18	1.07	0.73	0.95	0.53
Na_2O	2.58	2.51	2.47	2.60	2.49	2.59	2.77	2.40	2.57	2.71	2.19	2.35	2.52	2.50	2.44	2.39	2.49	2.72	2.69	1.91	1.34	0.94
K_2O	5.84	6.46	5.98	5.74	5.99	5.73	5.87	6.02	5.87	5.38	6.41	6.37	6.02	5.83	7.31	6.12	5.91	5.44	5.77	7.74	4.55	4.55
P_2O_5	0.09	0.09	0.07	0.07	0.08	0.08	0.15	0.14	0.17	0.09	0.17	0.15	0.15	0.07	0.13	0.07	0.08	0.06	0.06	0.12	0.17	0.15
LOI	0.81	1.08	1.17	0.95	n.d.	n.d.	n.d.	1.09	0.84	0.71	1.04	0.82	0.72	0.72	0.52	0.65	0.68	0.66	0.60			
SUM	99.6	98.5	100.2	99.1	98.5	98.5	98.2	99.0	100.5	100.2	100.4	100.5	98.4	99.9	99.2	100.4	100.8	99.1	99.9	100.7	100.4	101.2
Ba	398	494	404	274	400	457	419	406	572	312	464	458	369	369	457	369	360	534	540	679	497	413
Co	3	3	2	2	2	1	3	0	3	4	3	3	3	0	2	5	2	0	5	15	22	19
Cr	34	154	67	22	31	50	25	44	15	14	21	22	43	52	82	52	49	22	18	91	132	126
Cu	0	9	5	0	2	2	0	0	0	0	0	0	0	3	3	5	3	0	1	4	0	3
Ga	20	16	19	16	19	20	22	21	11	14	7	10	16	21	19	20	18	12	10	14	20	16
Nb	22	15	20	19	21	18	24	19	28	20	17	16	11	13	14	15	10	30	31	40	13	12
Ni	14	371	196	11	14	141	10	127	3	0	2	0	23	88	260	39	159	4	1	30	67	62
Pb	47	59	49	46	45	52	42	44	33	34	51	38	42	41	45	32	36	51	52	56	7	10
Rb	261	301	263	282	260	267	306	294	236	238	240	246	241	260	308	273	258	209	219	481	287	458
Sc	7	7	2	10	6	5	11	9	6	4	6	0	9	9	7	4	11	8	5	11	22	16
Sr	78	94	80	64	74	85	78	82	99	81	96	94	90	88	93	91	94	96	94	102	61	34
Th	30	64	32	41	34	35	33	31	36	32	42	38	73	66	60	59	74	44	34	14	2	7
U	11	13	7	8	7	7	7	9	5	10	7	3	3	6	8	12	7	14	8	18	6	0
V	16	12	18	9	9	4	12	15	14	16	14	11	16	12	15	8	14	12	7	103	214	203
Y	48	77	54	51	49	48	30	36	52	46	33	38	37	28	41	30	29	67	43	33	36	28
Zn	47	53	52	51	54	49	64	62	55	51	48	49	40	38	36	40	37	33	32	126	173	203
Zr	169	253	175	162	177	163	209	202	229	162	206	201	236	241	286	233	237	177	171	243	179	171
La	71.6	103	90.1	62.8	129	84.9	64.5	92.8	n.d.	n.d.	n.d.	n.d.	155	128	212	197	225	n.d.	n.d.	n.d.	n.d.	n.d.
Ce	147	205	181	136	266	171	131	186	n.d.	n.d.	n.d.	n.d.	282	241	395	383	427	n.d.	n.d.	n.d.	n.d.	n.d.
Nd	66.8	80.7	78.3	64.0	79.5	66.7	51.2	71.2	n.d.	n.d.	n.d.	n.d.	131	86.1	101	103	112	n.d.	n.d.	n.d.	n.d.	n.d.
Sm	14.0	18.3	17.0	14.5	16.2	14.5	10.4	14.7	n.d.	n.d.	n.d.	n.d.	21.4	15.0	16.3	17.0	18.3	n.d.	n.d.	n.d.	n.d.	n.d.
Eu	0.9	1.1	1.2	0.6	0.8	1.2	0.8	1.0	n.d.	n.d.	n.d.	n.d.	1.2	0.7	0.8	0.8	0.8	n.d.	n.d.	n.d.	n.d.	n.d.
Gd	9.8	13.5	12.1	10.0	11.6	10.6	7.6	9.6	n.d.	n.d.	n.d.	n.d.	10.8	8.0	10.0	9.9	10.9	n.d.	n.d.	n.d.	n.d.	n.d.
Dy	7.2	9.9	8.9	7.3	9.0	8.0	5.5	6.2	n.d.	n.d.	n.d.	n.d.	6.9	3.7	7.8	6.1	6.7	n.d.	n.d.	n.d.	n.d.	n.d.
Er	3.5	4.7	4.7	3.0	4.3	3.8	2.2	2.5	n.d.	n.d.	n.d.	n.d.	2.4	1.3	3.9	2.7	3.0	n.d.	n.d.	n.d.	n.d.	n.d.
Yb	2.6	3.9	3.7	2.2	3.6	3.1	1.4	2.0	n.d.	n.d.	n.d.	n.d.	1.8	0.9	3.7	2.3	2.5	n.d.	n.d.	n.d.	n.d.	n.d.
Lu	0.4	0.5	0.5	0.4	0.6	0.4	0.2	0.3	n.d.	n.d.	n.d.	n.d.	0.2	0.1	0.6	0.4	0.4	n.d.	n.d.	n.d.	n.d.	n.d.
Eu/Eu*	0.23	0.21	0.25	0.15	0.17	0.30	0.29	0.27					0.23	0.19	0.20	0.20	0.18					
La/Yb	19	18	16	19	24	18	31	31					58	96	39	58	61					
Rb/Sr	3.35	3.20	3.29	4.41	3.51	3.14	3.92	3.59	2.38	2.94	2.50	2.62	2.68	2.95	3.31	3.00	2.74	2.18	2.33	4.72	4.70	13.47

Table 3
Strontium, Nd and Pb isotope composition of leucogranites ON and OS.

Sample	S56	S60	S61	S63	S65	S66	S67	S72	S77	S78
$^{87}Sr/^{86}Sr_{(m)}$	0.782837	0.804475	0.785804	0.793539	0.786140	0.767252	0.769526	0.778704	0.771454	0.767351
Error	0.000007	0.000008	0.000007	0.000007	0.000007	0.000007	0.000006	0.000005	0.000005	0.000006
$^{87}Sr/^{86}Sr_{(i)}$	0.712202	0.711932	0.711500	0.711115	0.710410	0.711146	0.707649	0.709327	0.708408	0.709885
$^{87}Rb/^{86}Sr$	9.76	12.8	10.3	11.4	10.5	7.75	8.55	9.58	8.71	7.94
$^{143}Nd/^{144}Nd_{(m)}$	0.512173	0.512175	0.512166	0.512131	0.512143	0.511981	0.511966	0.511972	0.511989	0.511968
Error	0.000001	0.000002	0.000001	0.000001	0.000002	0.000001	0.000002	0.000002	0.000001	0.000002
$^{143}Nd/^{144}Nd_{(i)}$	0.511746	0.511714	0.511751	0.511718	0.511724	0.511670	0.511636	0.511666	0.511676	0.511658
$^{147}Sm/^{144}Nd$	0.127	0.137	0.123	0.123	0.125	0.099	0.105	0.098	0.100	0.099
$\varepsilon Nd_{(i)}$	−4.6	−5.3	−4.5	−5.2	−5.1	−6.1	−6.6	−6.1	−5.9	−6.2
T DM	1.5	1.7	1.5	1.6	1.6	1.4	1.5	1.4	1.4	1.5
$^{206}Pb/^{204}Pb$	18.57	18.60	18.56	18.52	18.51	18.68	19.13	n.d.	18.71	n.d.
$^{207}Pb/^{204}Pb$	15.66	15.67	15.66	15.63	15.67	15.68	15.69	n.d.	15.69	n.d.
$^{208}Pb/^{204}Pb$	38.13	38.09	38.11	38.08	38.12	38.66	38.31	n.d.	38.43	n.d.

Uncertainties in the $^{87}Sr/^{86}Sr$ and $^{143}Nd/^{144}Nd$ ratios are 2 σ (mean) errors in the last digit. εNd values are calculated relative to CHUR according to Jacobsen and Wasserburg (1980). Depleted mantle Nd model ages (T DM) are calculated according to Michard et al. (1985). m, measured; i, initial calculated for an age of 508 Ma. Samples S56 to S78 are from the study by Haack et al. (1980, 1982).

leucogranites are in excellent agreement with Nd model ages from metasedimentary xenoliths and metasediments from the Kuiseb formation which also cluster around 1.5 Ga (McDermott and Hawkesworth, 1990; Jung, 2005). The leucogranites have high $\delta^{18}O$ in excess of 13‰ (Haack et al., 1982) which also argue in favor of a pelitic source (Jung et al., 1999).

The granites from OS have moderately unradiogenic εNd values between −4.5 and −5.3, whereas for granites from ON εNd ranges from −5.8 to −6.6 similar to the values found in the xenoliths from the OGMC. The lack of correlation trends in Sr and Nd isotope space between the granites and surrounding country rocks (Fig. 7) indicates that AFC processes among the granites and older crust have not contributed to the isotope composition of the granites. Both granites are heterogeneous in their common Pb isotopic signature but define two distinct groups in $^{208}Pb/^{204}Pb$ vs. $^{206}Pb/^{204}Pb$, $^{207}Pb/^{204}Pb$ vs. $^{206}Pb/^{204}Pb$ and $^{87}Sr/^{86}Sr_{(init.)}$ vs. $^{208}Pb/^{204}Pb$ (Figs. 7 and 14). Granites from OS show a clear connection to the metasedimentary xenoliths from the OGMC whereas samples from ON correlate with the metasedimentary rocks from the OGMC. This observation may imply that both granite suites are generated from distinct metasedimentary sources.

7.3. Melting temperatures

Calculation of zircon and monazite saturation temperatures (Watson and Harrison, 1983; Montel, 1993) may be used to estimate the temperature of formation and evolution of granitic magmas. Internally consistent results are expected only if (1) chemical equilibrium prevailed during melting or crystallization, (2) the dissolution rate of the accessory mineral was fast relative to the melting event, (3) zircon and monazite were not present as inclusions in residual minerals during melting or fractional crystallization, (4) accessory minerals control the budget of trace elements, and (5) the whole rock composition approximates a frozen melt (Miller et al., 2003; Jung and Pfänder, 2007). Zircon and monazite saturation temperatures are given in Table 4. Apparently inheritance of zircon cores results in overestimation of the whole rock Zr content and the calculated zircon saturation temperature. However, this effect is

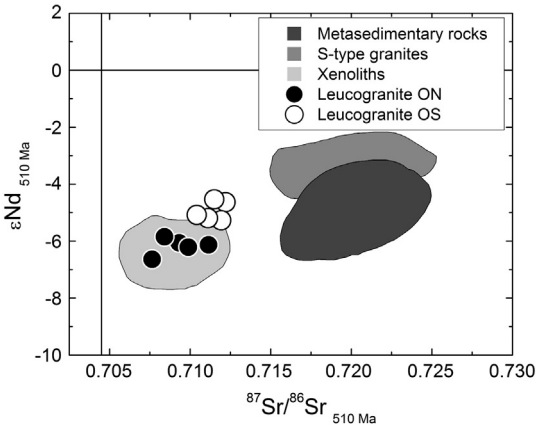

Fig. 7. Initial $^{87}Sr/^{86}Sr$ vs. initial εNd diagram for the Okombahe leucogranites. Fields for metasedimentary xenoliths, S-type granites and metasedimentary rocks are taken from Jung (2005).

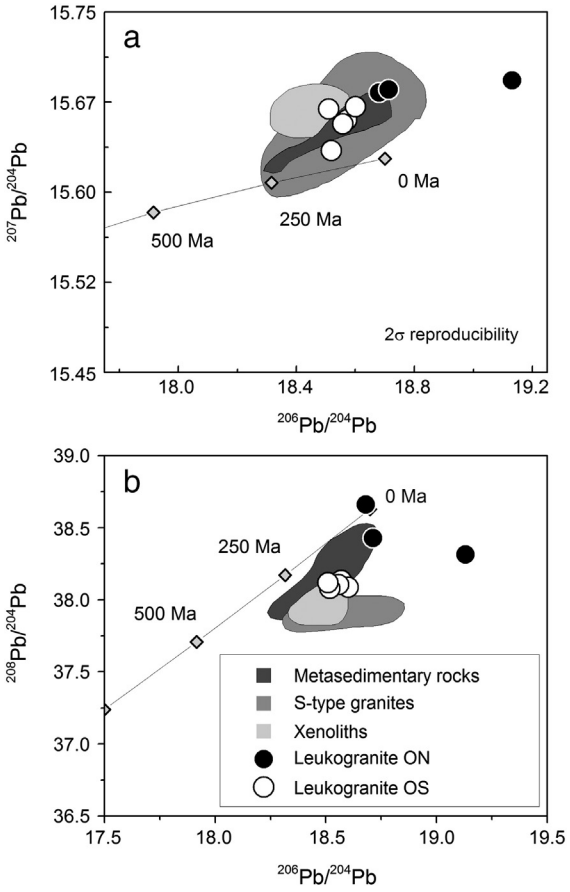

Fig. 8. (a) Plot of $^{207}Pb/^{204}Pb$ and (b) $^{208}Pb/^{204}Pb$ vs. $^{206}Pb/^{204}Pb$ isotope ratios of leached K-feldspar from leucogranites from ON and OS. Data for metasedimentary xenoliths, S-type granites and metasedimentary rock data are taken from Jung (2005). The curves show average crustal Pb growth according to Stacey and Kramers (1975). Tick marks represent 250 Ma intervals.

Please cite this article as: Paul, A., et al., Petrogenesis of synorogenic high-temperature leucogranites (Damara orogen, Namibia): Constraints from U–Pb monazite ages and Nd, S..., Gondwana Research (2013), http://dx.doi.org/10.1016/j.gr.2013.06.008

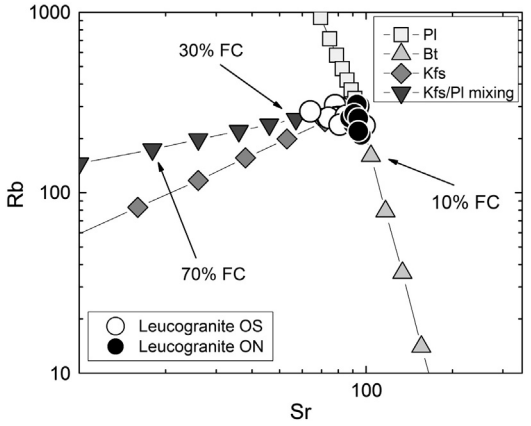

Fig. 9. Variation in Rb, Sr and Ba concentrations for leucogranites from ON and OS. Mineral vectors calculated with partition coefficients from Bea et al. (1994) for biotite, plagioclase and K-feldspar. Compositional trends from OS and ON suggest 25% and 10% fractional crystallization, respectively. Fractionation trend of OS is best explained with a 1:1 aspect ratio of plagioclase and K-feldspar. The trend displayed by samples from ON can be explained by less than 10% fractionation of biotite.

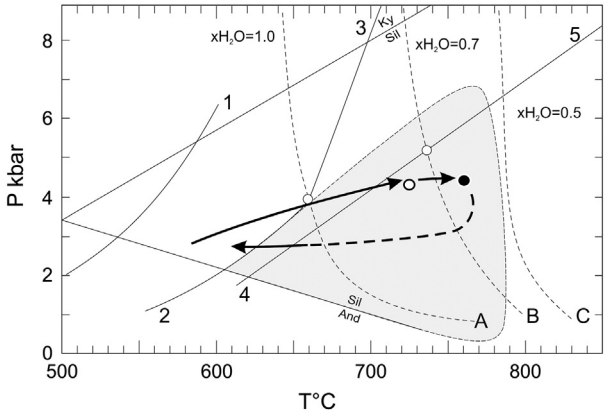

Fig. 11. P–T diagram showing estimated pressure and temperature conditions of metasedimentary country rocks as an indicator of peak metamorphic conditions at the level of intrusion. Aluminum silicate triple-point from Holdaway (1971). (1) Crd = Chl + And + Qtz (Seifert and Schreyer, 1970) (2) Ms + Ab + Qtz ↔ Kfs + As + V (Spear et al., 1999; NaKFMASH system); (3) Ms + Ab + Qtz ↔ As + Kfs + melt (Spear et al., 1999; NaKFMASH system); (4) Bt + Sil + Qtz ↔ Grt + Crd + Kfs + V (Spear et al., 1999; NaKFMASH system); (5) Bt + Sil + Qtz ↔ Grt + Crd + Kfs + melt (Spear et al., 1999; NaKFMASH system), wet melting curves A, B and C from Johannes (1985). Black arrow is the proposed metamorphic evolution inferred from conditions reached in the Oetmoed Granite–Migmatite Complex (Jung et al., 1999). Shaded area indicates possible P–T conditions.

usually small because a core the size of half the grain radius corresponds to only 1/8 of its mass. Moreover, zircon saturation temperatures correlate with those calculated for the monazites, which are unzoned and do not contain any inherited cores. Inherited zircon cores therefore do not play a significant role. Both zircon and monazite saturation temperatures correlate negatively with SiO_2, which indicates saturation in Zr and LREE early during magmatic evolution. The high saturation temperatures of 800 to 840 °C are in agreement with temperatures assumed for crustal melting (Clemens and Vielzeuf, 1987).

Pressure–temperature estimates for the country rocks are ca. 750 °C (Table 5) at 5 kbar, corresponding to a depth of ca. 19 km. Considering

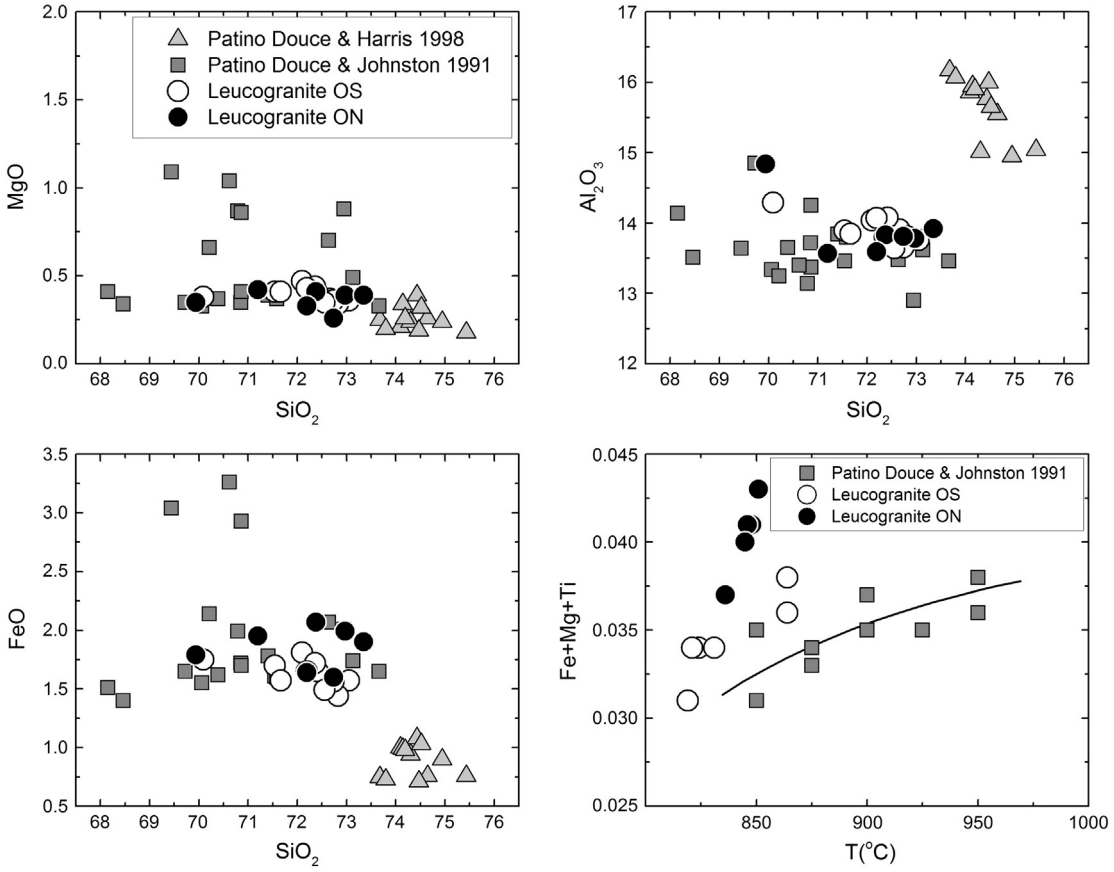

Fig. 10. Comparison of experimental data for pelite melting (Patiño Douce and Johnston, 1991; Patiño Douce and Harris, 1998) with concentrations of leucogranites from ON and OS.

Please cite this article as: Paul, A., et al., Petrogenesis of synorogenic high-temperature leucogranites (Damara orogen, Namibia): Constraints from U–Pb monazite ages and Nd, S..., Gondwana Research (2013), http://dx.doi.org/10.1016/j.gr.2013.06.008

Table 4
Calculated saturation temperatures (°C) for leucogranites from Okombahe, Namibia.

Sample	LREE	Zr	Sample	LREE	Zr
S57	854	831	S67	877	828
S56	810	799	S66	866	825
S58	824	801	S72	867	838
S60	822	794	S77	869	825
S61	829	804	S78	874	826
S62	812	798	ON1	823	796
S65	832	814	ON2	821	793
S63	830	813			
OS1	836	825			
OS2	804	792			
OS3	817	817			
OS4	825	810			

Inferred water content for application of the LREE sat. equation is 4 wt.% H_2O (Montel, 1993).

an average geothermal gradient of 15 °C/km, temperatures of 850 °C for the generation of the leucogranites are achieved at ca. 26 km depth equivalent to a pressure of ca. 7 kbar. The temperature of ~850 °C reached at this level is sufficient to cause biotite dehydration melting which is considered to yield leucogranitic melts at about 850 °C (Le Breton and Thompson, 1988; Vielzeuf and Holloway, 1988; Vielzeuf and Montel, 1994; Montel and Vielzeuf, 1997; among many others).

While the inferred geothermal gradient may be subject to discussion, it is evident from previous investigations (Haack et al., 1983) that heat producing lower crustal units contributed 100–150 °C excess temperature to the thermal regime of the Central Damara orogen. In conjunction with high temperature metamorphism, this level of excess heat production is probably sufficient to increase temperatures from peak metamorphic conditions (700–750 °C, Jung and Mezger, 2003) to temperatures where biotite dehydration melting occurs (>850 °C) at lower levels. The high Zr saturation temperatures obtained from the most primitive samples (OS = 835 °C; ON = 843 °C) are in good agreement with the inferred conditions for biotite dehydration melting and facilitate melting without additional heat input or adiabatic decompression. Pressure estimates can be derived from Qz–Ab–Or systematics. It is evident from Fig. 12 that the majority of the leucogranites from both localities were generated at pressures less than 7 kbar corresponding to depths of less than 26 km. The most felsic samples record emplacement pressures of ca. 4 kbar corresponding to depths of ca. 19 km.

Partial melting of metasedimentary rocks producing mobile granitic magmas is related to incongruent biotite breakdown under fluid absent conditions (Le Breton and Thompson, 1988). Melting experiments on Al-rich metapelites of the Damara belt (Ward et al., 2008) have shown that felsic melts and peritectic garnet are produced at high temperatures (800–850 °C). Residual peritectic garnet will control the HREE abundances (Taylor and Stevens, 2010) and may be responsible for the large HREE fractionation in the leucogranites of OS and ON. Model calculations using batch and fractional melting equations applied

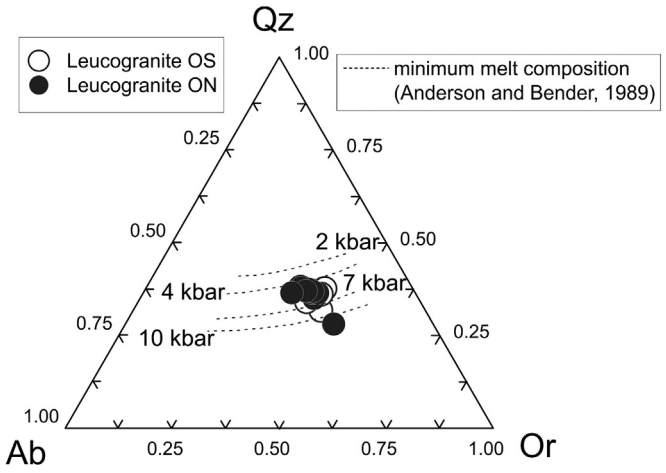

Fig. 12. Normative Qz, Ab and Or composition of the leucogranites OS and ON relative to experimental H_2O-saturated minimum melt composition (Anderson and Bender, 1989).

on Al-rich metapelites from the Oetmoed Granite–Migmatite Complex demonstrate that the modal composition of these metapelites is close to the optimum melting mode (Patiño Douce and Johnston, 1991). Models were performed for the trace elements Rb, Ba, and Sr. In Fig. 13, the bulk distribution coefficients for Sr = 1.5 and Rb = 0.5 (path A) or, alternatively Sr = 1.5 and Rb = 0.1 (path B) account for different behavior of Rb during melting. The chemical composition of metasedimentary rocks is taken from the OGMC (Jung et al., 2000b). In Fig. 13 the melt composition obtained by partial melting is enriched in Rb and depleted in Sr, relative to the source rock. The trend of the samples is parallel to the trend of partial melting. This observation demonstrates that the observed concentrations of trace elements are more likely controlled by partial melting and not by fractional crystallization processes. In order to obtain the trace element abundances observed in the leucogranites, melt fractions in the range 10–50% are needed. 10% partial melt is certainly a lower limit; however, these results are compatible with the observations by Clemens and Vielzeuf (1987) on the partial melting behavior of metapelites under lower crustal conditions.

8. Conclusions

Two suites of leucogranites in the Damara orogen formed during peak metamorphism. High temperature conditions at lower crustal levels led to biotite dehydration melting of pelitic material during maximum thickening of the continental crust. Modeling crystal fractionation processes suggests low extents of fractionational crystallization. Sr and Nd isotope data provide no evidence for crustal assimilation processes. The granites are therefore interpreted to represent near-minimum melt compositions that have efficiently segregated from their sources.

Table 5
Calculated Na-in-Crd temperatures for metasediments from Leucogranites OS and ON.

Sample		MS1-1	MS1-2	MS1-3	
	Na p.f.u.	0.0854	0.0835	0.0753	Avg. T°C
Mirwald (1986)	Temp (°C)	645	650	673	656
Mirwald et al. (2008) (High xH_2O, low Na_2O)	Temp (°C)	644	649	671	655
Mirwald et al. (2008) (Low xH_2O, high Na_2O)	Temp (°C)	714	719	744	726
Wyhlidal et al. (2007)	Temp (°C)	727	731	748	735
		MS2-1	MS2-2	MS2-3	
	Na p.f.u.	0.0334	0.0396	0.0435	avg. T°C
Mirwald (1986)	Temp (°C)	791	774	763	776
Mirwald et al. (2008) (High xH_2O, low Na_2O)	Temp (°C)	785	768	757	770
Mirwald et al. (2008) (Low xH_2O, high Na_2O)	Temp (°C)	873	854	842	856
Wyhlidal et al. (2007)	Temp (°C)	837	824	815	825

Please cite this article as: Paul, A., et al., Petrogenesis of synorogenic high-temperature leucogranites (Damara orogen, Namibia): Constraints from U–Pb monazite ages and Nd, S..., Gondwana Research (2013), http://dx.doi.org/10.1016/j.gr.2013.06.008

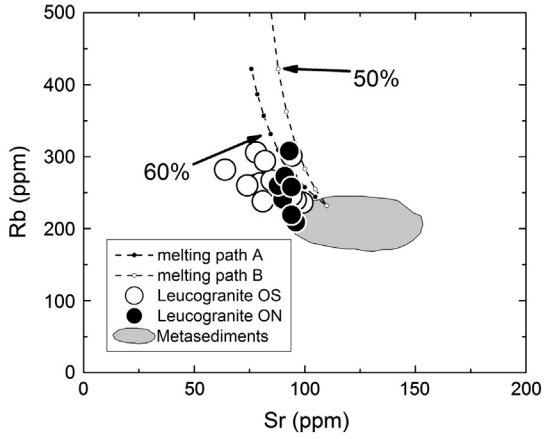

Fig. 13. Variation in Rb and Sr concentration for two different batch melting models using bulk KDs of 1.5 (Sr) and 0.5 or 0.1 (Rb) to reflect biotite dehydration melting with residual plagioclase (see text). Melt fractions required to generate leucogranites from Damara metasedimentary rocks are in the range of 30–50%.

Relative to other S-type leucogranites from the orogen, the unradiogenic, but still crustal Sr and Nd isotope compositions of the leucogranites imply that the source rocks had an isotopic composition distinct from those inferred for other S-type leucogranites in the northern Central Zone. The Sr, Nd and Pb isotope ratios of the leucogranites overlap with values from metasedimentary xenoliths found in other S-type granites from the Damara orogen, suggesting a metapelitic source. High temperatures of ca. 850 °C are recorded by zircon and monazite saturation thermometers which are in good agreement with conditions necessary for the formation of leucogranitic melts by biotite dehydration melting of metasedimentary rocks under water-undersaturated conditions. Pressure and temperature estimates indicate that crustal thickening alone is sufficient to cause widespread biotite dehydration melting under fluid absent conditions, leading to internal crustal recycling with no external heat input by the mantle or excessive addition of fluids. The results from this study also show that upper mantle-derived melts did not contribute to the heat budget of the crust and hence to partial melting. Instead, crustal thickening and internal heating seem to be sufficient to generate leucogranitic melts at lower crustal conditions.

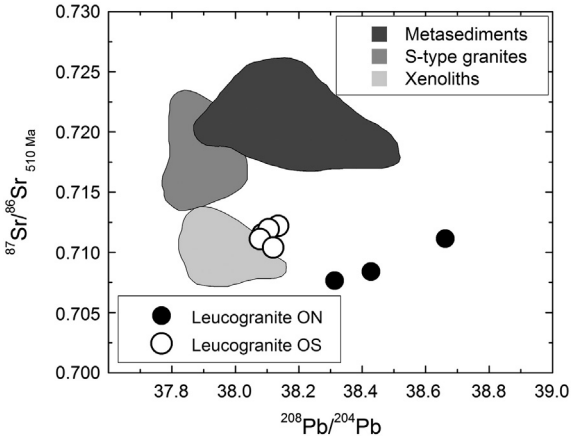

Fig. 14. Plot of $^{208}Pb/^{204}Pb$ isotope ratios vs. initial $^{87}Sr/^{86}Sr$ ratios for S-type granites, metasedimentary rocks, metasedimentary xenoliths from Oetmoed (central Damara orogen, Namibia, Jung, 2005).

Acknowledgments

H. Baier of the Westfälische Wilhelms Universität Münster is thanked for assistance during chemical separation and during measurements of Sr, Nd and Pb isotopes. E. Thun, S. Heidrich and P. Stutz are thanked for assistance during XFA and EMP analyses and preparation of thin sections at the Universität Hamburg. We thank the reviewers for constructive comments which improved the paper.

References

Anderson, J.L., Bender, E.E., 1989. Nature and origin of Proterozoic A-type granitic magmatism in the southwestern United States of America. Lithos 23, 19–52.
Barbarin, B., 1996. Genesis of the two main types of peraluminous granitoids. Geology 24, 295–298.
Bea, F., Pereira, M.D., Stroh, A., 1994. Mineral/leucosome trace-element partitioning in a peraluminous migmatite (a laser ablation-ICP-MS study). Chemical Geology 117, 291–312.
Boynton, W., 1984. Geochemistry of rare-earth elements: meteorite studies. In: Henderson, P. (Ed.), Rare Earth Element Geochemistry. Elsevier, Amsterdam, pp. 63–114.
Cameron, A.E., Smith, D.H., Walker, R.L., 1969. Mass spectrometry of nanogram-size samples of lead. Analytical Chemistry 41, 525–526.
Clemens, J.D., Vielzeuf, D., 1987. Constraints on melting and magma production in the crust. Earth and Planetary Science Letters 86, 287–306.
Clemens, J.D., Wall, V.J., 1988. Controls on the mineralogy of S-type volcanic and plutonic rocks. Lithos 21, 53–66.
Collins, W.J., 1996. Lachlan Fold Belts granitoids: products of three-component mixing. Transactions of the Royal Society of Edinburgh: Earth Sciences 87, 171–181.
Copeland, P., Parrish, R.R., Harrison, T.M., 1988. Identification of inherited radiogenic Pb in monazite and its implications for U–Pb systematics. Nature 333, 760–763.
Gerstenberger, H., Haase, G., 1997. A highly effective emitter substance for mass spectrometric Pb isotope ratio determinations. Chemical Geology 136, 309–312.
Gray, D., Foster, D., Goscombe, B., Passchier, C., Trouw, R., 2006. 40Ar/39Ar thermochronology of the Pan-African Damara Orogen, Namibia, with implications for tectonothermal and geodynamic evolution. Precambrian Research 150, 49–72.
Guo, Z., Wilson, M., 2011. The Himalayan leucogranites: constraints on the nature of their crustal source region and geodynamic setting. Gondwana Research 22, 360–376.
Haack, U., Gohn, E., Klein, J., 1980. Rb/Sr ages of granitic rocks along the middle reaches of the Omaruru River. Contributions to Mineralogy and Petrology 74, 349–360.
Haack, U., Hoefs, J., Gohn, E., 1982. Constraints on the origin of Damaran granites by Rb/Sr and 6180 data. Contributions to Mineralogy and Petrology 79, 279–289.
Haack, U., Gohn, E., Hartmann, O., 1983. Radiogenic heat generation in Damaran rocks. Special Publication Geological Society of South Africa 225–231.
Harris, N., Inger, S., 1992. Trace element modelling of pelite-derived granites. Contributions to Mineralogy and Petrology 110, 46–56.
Harris, N., Inger, S., Massey, J., 1993. The role of fluids in the formation of high Himalayan leucogranites. In: Treloar, P.J., Searle, M.P. (Eds.), Himalayan Tectonics. Geological Society of London Special Publications, 74, pp. 391–400.
Hartmann, O., Hoffer, E., Haack, U., 1983. Regional metamorphism in the Damara orogen: interaction of crustal motion and heat transfer. Special Publication Geological Society of South Africa 11, 233–241.
Holdaway, M.J., 1971. Stability of andalusite and the aluminium silicate phase diagram. American Journal of Science 271, 97–131.
Jacobsen, S., Wasserburg, G., 1980. Sm–Nd isotopic evolution of chondrites. Earth and Planetary Science Letters 50, 139–155.
Johannes, W., 1985. The significance of experimental studies for the formation of migmatites. In: Ashworth, J.R. (Ed.), Migmatites. Blackie, Glasgow and London, p. 41.
Johannsen, A., 1932. A Descriptive Petrography of Igneous Rocks, 2. University of Chicago Press, pp. 120–124.
Jung, S., 2000. High-temperature, low/medium-pressure clockwise P–T paths and melting in the development of regional migmatites: the role of crustal thickening and repeated plutonism. Geological Journal 35, 345–359.
Jung, S., 2005. Isotopic equilibrium/disequilibrium in granites, metasedimentary rocks and migmatites (Damara orogen, Namibia)—a consequence of polymetamorphism and melting. Lithos 84, 168–184.
Jung, S., Hellebrand, E., 2006. Trace element fractionation during high-grade metamorphism and crustal melting-constraints from ion microprobe data of metapelitic, migmatitic and igneous garnets and implications for Sm–Nd garnet chronology. Lithos 87, 193–213.
Jung, S., Mezger, K., 2001. Geochronology in migmatites — a Sm–Nd, U–Pb and Rb–Sr study from the Proterozoic Damara belt (Namibia): implications for polyphase development of migmatites in high grade terranes. Journal of Metamorphic Geology 19, 77–97.
Jung, S., Mezger, K., 2003. Petrology of basement-dominated terranes: I. Regional metamorphic T–t path from U–Pb monazite and Sm–Nd garnet geochronology (Central Damara orogen, Namibia). Chemical Geology 198, 223–247.
Jung, S., Pfänder, J.A., 2007. Source composition and melting temperatures of orogenic granitoids: constraints from CaO/Na_2O, Al_2O_3/TiO_2 and accessory mineral saturation thermometry. European Journal of Mineralogy 19, 859–870.
Jung, S., Mezger, K., Hoernes, S., 1998a. Petrology and geochemistry of syn- to post-collisional metaluminous A-type granites — major and trace element and Nd–Sr–Pb–O-isotope study from the Proterozoic Damara Belt, Namibia. Lithos 45, 147–175.

Jung, S., Mezger, K., Masberg, P., Hoffer, E., Hoernes, S., 1998b. Petrology of an intrusion-related high-grade migmatite: implications for partial melting of metasedimentary rocks and leucosome-forming processes. Journal of Metamorphic Geology 16-3, 425–445.
Jung, S., Hoernes, S., Masberg, P., Hoffer, E., 1999. The petrogenesis of some migmatites and granites (Central Damara Orogen, Namibia): evidence for disequilibrium melting, wall-rock contamination and crystal fractionation. Journal of Petrology 40, 1241–1269.
Jung, S., Hoernes, S., Mezger, K., 2000a. Geochronology and petrogenesis of Pan-African, syn-tectonic, S-type and post-tectonic A-type granite (Namibia): products of melting of crustal sources, fractional crystallization and wall rock entrainment. Lithos 50, 259–287.
Jung, S., Hoernes, S., Mezger, K., 2000b. Geochronology and petrology of migmatites from the Proterozoic Damara Belt — importance of episodic fluid-present disequilibrium melting and consequences for granite petrology. Lithos 51, 153–179.
Jung, S., Mezger, K., Hoernes, S., 2001. Trace element and isotopic (Sr, Nd, Pb, O) arguments for a mid-crustal origin of Pan-African garnet-bearing S-type granites from the Damara orogen (Namibia). Precambrian Research 110, 325–355.
Jung, S., Masberg, P., Mihm, D., Hoernes, S., 2009. Partial melting of diverse crustal sources — constraints from Sr–Nd–O isotope compositions of quartz diorite–granodiorite–leucogranite associations (Kaoko Belt, Namibia). Lithos 111, 236–251.
Kretz, R., 1983. Symbols of rock-forming minerals. American Mineralogist 68, 277–279.
Le Breton, N., Thompson, A., 1988. Fluid-absent (dehydration) melting of biotite in metapelites in the early stages of crustal anatexis. Contributions to Mineralogy and Petrology 99, 226–237.
Masberg, H., Hoffer, E., Hoernes, S., 1992. Microfabrics indicating granulite-facies metamorphism in the low-pressure central Damara Orogen, Namibia. Precambrian Research 55, 243–257.
Masberg, P., Mihm, D., Jung, S., 2005. Major and trace element and isotopic (Sr, Nd, O) constraints for Pan-African crustally contaminated grey granite gneisses from the southern Kaoko belt, Namibia. Lithos 84, 25–50.
Mattinson, J.M., 1973. Anomalous isotopic composition of lead in young zircons. Carnegie Institution of Washington Yearbook 72, 613–616.
Mattinson, J.M., 1986. Geochronology of high-pressure–low-temperature Franciscan metabasites: a new approach using the U–Pb system. Geological Society of America, Memorial 164, 95–105.
McDermott, F., Hawkesworth, C.J., 1990. Intracrustal recycling and upper-crustal evolution: a case study from the Pan-African Damara mobile belt, central Namibia. Chemical Geology 83, 263–280.
McDermott, F., Harris, N.B., Hawkesworth, C.J., 1996. Geochemical constraints on crustal anatexis: a case study from the Pan-African Damara granitoids of Namibia. Contributions to Mineralogy and Petrology 123, 406–423.
Michard, A., Guriet, P., Soudant, M., Albarède, F., 1985. Nd isotopes in French Phanerozoic shales: external vs. internal aspects of crustal evolution. Geochimica et Cosmochimica Acta 49, 601–610.
Milisenda, C., Liew, T., Hofmann, A., Köhler, H., 1994. Nd isotopic mapping of the Sri Lanka basement: update, and additional constraints from Sr isotopes. Precambrian Research 66, 95–110.
Miller, R.McG., 1983. The Pan-African Damara orogen of Namibia. In: Miller, R. McG (Ed.), The Damara Orogen. Special Publications of the Geological Society of South Africa.
Miller, C.F., 1985. Are strongly peraluminous magmas derived from pelitic sedimentary sources. Journal of Geology 93, 673–689.
Miller, R.McG., 2008. The Geology of Namibia, vol 1–3. Ministry of Mines and Energy, Geological Survey, Windhoek.
Miller, C.F., Mittlefehldt, D.W., 1982. Depletion of light rare-earth elements in felsic magmas. Geology 10, 129–133.
Miller, C.F., McDowell, S., Mapes, R., 2003. Hot and cold granites? Implications of zircon saturation temperatures and preservation of inheritance. Geology 6, 529–532.
Mirwald, P.W., 1986. Fortschritte der Mineralogie 64, 119.
Mirwald, P.W., Scola, M., Tropper, P., 2008. Experimental study on the incorporation of Na in Mg-cordierite in the presence of different fluids (Na(OH), NaCl-H_2O, albite-H_2O). Geophysical Research Abstracts 10A, 04149.
Montel, J.M., 1993. A model for monazite/melt equilibrium and application to the generation of granitic magmas. Chemical Geology 110, 127–146.
Montel, J.M., Vielzeuf, D., 1997. Partial melting of metagreywackes. Part II. Compositions of minerals and melts. Contributions to Mineralogy and Petrology 128, 176–196.
Parada, M.A., Nyström, J.O., Levi, B., 1997. Multiple sources for the Coastal Batholith of central Chile (31–34°S): geochemical and Sr–Nd isotopic evidence and tectonic implications. Lithos 46, 505–521.
Patiño Douce, A.E., Harris, N., 1998. Experimental constraints on Himalayan anatexis. Journal of Petrology 39 (4), 689–710.
Patiño Douce, A.E., Johnston, A., 1991. Phase equilibria and melt productivity in the pelitic system: implications for the origin of peraluminous granitoids and aluminous granulites. Contributions to Mineralogy and Petrology 107, 202–218.
Romer, R.L., Heinrich, W., Schröder-Smeibidl, B., Meixner, A., Fischer, C.O., Schulz, C., 2005. Elemental dispersion and stable isotope fractionation during reactive fluid-flow and fluid immiscibility in the Bufa del Diente aureole, NE-Mexico: evidence from radiographies and Li, B, Sr, Nd, and Pb isotope systematics. Contributions to Mineralogy and Petrology 149, 400–429.
Rötzler, J., Romer, R.L., 2001. P-T-t evolution of ultrahigh-temperature granulites from the Saxon Granulite Massif, Germany. Part I: Petrology. Journal of Petrology 42 (11), 1995–2013.
Schärer, U., 1984. The effect of initial 230Th disequilibrium on young U–Pb ages: the Makalu case, Himalaya. Earth and Planetary Science Letters 67, 191–204.
Seifert, F., Schreyer, W., 1970. Lower temperature stability limit of Mg cordierite in the range 1–7 kb water pressure: a redetermination. Contributions to Mineralogy and Petrology 27, 225–238.
Soesoo, A., 2000. Fractional crystallization of mantle derived melts as a mechanism for some I-type granite petrogenesis: an example from Lachlan Fold Belt, Australia. Journal of the Geological Society of London 157, 135–149.
Spear, F.S., Kohn, M.J., Cheney, J.T., 1999. P–T paths from anatectic pelites. Contributions to Mineralogy and Petrology 134, 17–32.
Stacey, J.S., Kramers, J.D., 1975. Approximation of terrestrial lead isotope evolution by a two-stage model. Earth and Planetary Science Letters 26, 207–221.
Taylor, J., Stevens, G., 2010. Selective entrainment of peritectic garnet into S-type granitic magmas: evidence from Archaean mid-crustal anatectites. Lithos 120, 277–292.
Tompson, A.B., 1982. Dehydration melting of pelitic rocks and the generation of H_2O-undersaturated granitic liquids. American Journal of Science 282, 1567–1595.
Vielzeuf, D., Holloway, J., 1988. Experimental determination of the fluid-absent melting relations in the pelitic system; consequences for crustal differentiation. Contributions to Mineralogy and Petrology 98, 257–276.
Vielzeuf, D., Montel, J.M., 1994. Partial melting of metagreywackes. Part I. Fluid-absent experiments and phase relationships. Contributions to Mineralogy and Petrology 117, 375–393.
Vielzeuf, D., Clemens, J.D., Pin, C., Moinet, E., 1990. Granites, granulites and crustal differentiation. In: Vielzeuf, D., Vidal, P. (Eds.), Granulites and Crustal Differentiation. Kluwer Academic Publishers, Dordrecht, pp. S. 59–85.
Ward, R., Stevens, G., Kisters, A., 2008. Fluid and deformation induced partial melting and melt volumes in low-temperature granulite-facies metasediments, Damara Belt, Namibia. Lithos 105, 253–271.
Watson, E.B., Harrison, T.M., 1983. Zircon saturation revisited: temperature and composition effects in a variety of crustal magma types. Earth and Planetary Science Letters 64, 295–304.
Wyhlidal, S., Thöny, W.F., Tropper, P., 2007. Supplement Geochimica et Cosmochimica Acta 71 (15 s), A1129.

Please cite this article as: Paul, A., et al., Petrogenesis of synorogenic high-temperature leucogranites (Damara orogen, Namibia): Constraints from U–Pb monazite ages and Nd, S..., Gondwana Research (2013), http://dx.doi.org/10.1016/j.gr.2013.06.008